CLIMATOLOGY

Unique thermal expansion properties of water key to the formation of sea ice on Earth

Fabien Roquet[1]*, David Ferreira[2], Romain Caneill[1], Daniel Schlesinger[3]†, Gurvan Madec[4]

The formation of sea ice in polar regions is possible because a salinity gradient or halocline keeps the water column stable despite intense cooling. Here, we demonstrate that a unique water property is central to the maintenance of the polar halocline, namely, that the thermal expansion coefficient (TEC) of seawater increases by one order of magnitude between polar and tropical regions. Using a fully coupled climate model, it is shown that, even with excess precipitations, sea ice would not form at all if the near-freezing temperature TEC was not well below its ocean average value. The leading order dependence of the TEC on temperature is essential to the coexistence of the mid/low-latitude thermally stratified and the high-latitude sea ice–covered oceans that characterize our planet. A key implication is that nonlinearities of water properties have a first-order impact on the global climate of Earth and possibly exoplanets.

INTRODUCTION

Most of what makes the water molecule H_2O so unique can be traced back to its structure with the V-shaped arrangement of hydrogen atoms around the oxygen atom and its electronic structure with two lone pairs giving rise to a strong polarity (*1*). Because of its polarity, a water molecule can form hydrogen bonds with neighboring molecules, adding cohesion within the liquid and making the heat capacity, the latent heat of fusion and of evaporation, or the surface tension of liquid water all exceptionally large. These properties explain why water is so central to the climate system on Earth (*2*).

As the hydrogen and oxygen atoms form a 104.5° angle, almost equal to the 109.5° angle found in a regular tetrahedron (*3*), water molecules can form open crystal structures where each water molecule is at the center of a tetrahedron formed by the neighboring molecules. This is precisely why liquid water is denser than ice near the freezing point.

This is also the reason why the thermal expansion coefficient (TEC) of seawater drops considerably near the freezing point. Here, we will show that the strong dependence of the TEC on temperature has a profound and generally overlooked influence on the formation of sea ice on Earth, on the general organization of the upper ocean stratification, and on vertical exchanges between the surface and deep layers of the ocean.

The TEC of liquid water

The TEC measures the relative variation of density caused by a unit change of temperature

$$\alpha = -\frac{1}{\rho}\frac{\partial \rho}{\partial \Theta}\bigg|_{S,p} \quad (1)$$

where ρ is the mass density, Θ is the conservative temperature, S is the absolute salinity, and p is the pressure. Note that the exact definition of TEC varies depending on the standard used to define the temperature or salinity properties. Here, we use the thermodynamic equation of seawater TEOS-10 standard (*4*); however, we stress that our results are independent of the standard used.

In a simple liquid (e.g., liquid argon or nitrogen) (*5*, *6*), the TEC is most commonly positive, i.e., its density monotonously decreases when temperature increases. However, pure liquid water has the rare property that, at standard pressure, it does not reach the maximum density at the freezing point but at a temperature of 4°C. This means that the TEC for liquid water is negative at temperatures below 4°C.

The implications of this negative TEC are well known for the stratification of the so-called dimictic lakes (*7*, *8*). In these lakes, the bottom is filled with the densest 4°C water year long and isolated from surface waters both in winter and in summer. Note, however, that very deep lakes may have a bottom temperature substantially lower than 4°C as the temperature of maximum density decreases with pressure, effectively limiting the depth of full overturn (*9*). The 4°C maximum density property enables the formation of ice at the surface, as only a surface layer of limited depth needs to be cooled down to drive freezing. It is much harder to freeze entirely the lake over wintertime, thus providing a safe habitat for species living in the lake.

The situation is fundamentally different for the oceans, because salt substantially modifies the physical properties of water. Dissolving salt in water increases the TEC of the solution at the same time as it lowers its freezing point (Fig. 1B). The structure of the water solvent in NaCl aqueous solutions is known to be modified in a similar way to that of water under enhanced pressure (*10*). Increasing salinity by 1 g kg^{-1} induces a similar rise in the TEC value as a 100-dbar pressure increase (Fig. 1A). Negative TEC values are found only for salinities below 25 g kg^{-1}, making it extremely rare to encounter except near cold estuaries. Thus, the mechanism promoting the formation of ice in freshwater lakes does not operate in the ocean. However, sea ice is forming on large areas of the polar ocean, and this study explores whether this could be related to patterns of TEC variations in the upper ocean.

Stratification control in the ocean

Polar regions are generally associated with excess precipitation over evaporation, freshening the upper ocean and forming a permanent halocline (*11*, *12*). In turn, the permanent halocline limits thermally

[1]Department of Marine Sciences, University of Gothenburg, 40530 Gothenburg, Sweden. [2]Department of Meteorology, University of Reading, Reading RG66ET, UK. [3]Department of Environmental Science and Bolin Centre for Climate Research, Stockholm University, 106 91 Stockholm, Sweden. [4]LOCEAN, Sorbonne Universités, UPMC, Paris, France.
*Corresponding author. Email: fabien.roquet@gu.se
†Present address: Environment and Health Administration, SLB-analys, Stockholm 104 20, Sweden.

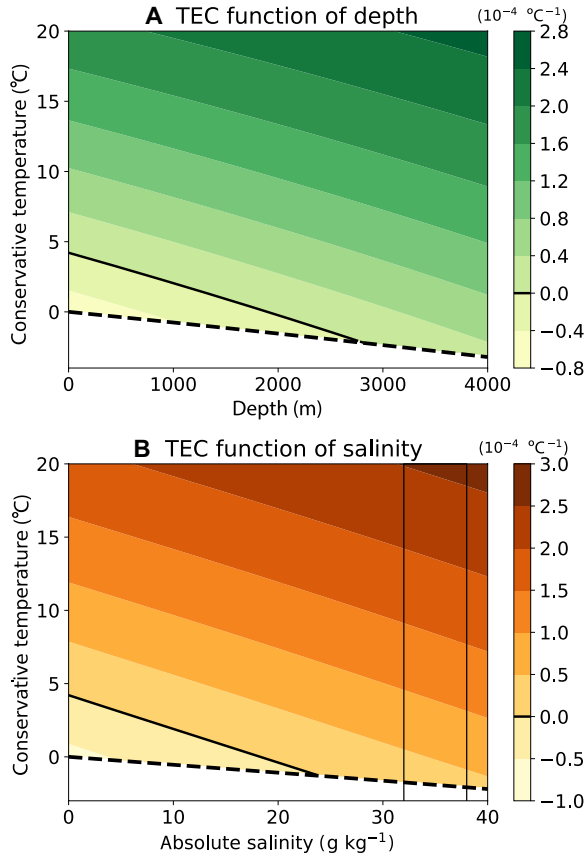

Fig. 1. Variation of the TEC with respect to temperature, salinity, and depth. (**A**) TEC function of temperature and depth for fresh water, i.e., at salinity $S = 0$ g kg^{-1}. Here, depth is taken proportional to pressure (1 m ≃ 1 dbar). (**B**) Variation of the TEC with respect to temperature and salinity at atmospheric pressure $p = 0$ dbar. The typical salinity range of seawater is indicated with light solid contours. The TEC decreases quasi-linearly with respect to temperature, pressure, and salinity. In both panels, the dashed line indicates the freezing point, while the solid line indicates where the TEC changes sign.

driven deep convection, thus promoting the formation of sea ice in polar regions. It has long been noted that sea ice formation occurs only in the presence of a halocline (*13*). It would seem natural to assume that the freshwater forcing alone explains why polar regions are stratified in salinity. However, the argument is somewhat incomplete and does not explain why the intense cooling is generally not able to wipe out the polar halocline.

The stratification is commonly quantified by the squared buoyancy frequency, $N^2 = -g\rho_z^\Theta/\rho$, where ρ^Θ is the potential density, g is the gravity acceleration, and the subscript z indicates the vertical derivative (*14*). The buoyancy frequency can be decomposed into the sum of temperature and salinity contributions

$$N^2 = N_\Theta^2 + N_S^2 \tag{2}$$

with $N_\Theta^2 = g\alpha\Theta_z$ and $N_S^2 = -g\beta S_z$. Here, $\beta = (\partial\rho/\partial S)\,|_{\Theta,p}/\rho$ defines the saline contraction coefficient, analogous to the TEC in Eq. 1 for salt.

Carmack (*13*) proposed to distinguish between the alpha ocean, where the upper ocean thermal stratification is stable ($N_\Theta^2 > 0$), and the beta ocean, where the haline stratification is stable ($N_S^2 > 0$). To avoid the ambiguity of this definition in regions where both thermal and haline stratifications are stable, we will define three regimes using the stratification control index (SCI) defined as $\mathrm{SCI} = (N_\Theta^2 - N_S^2)/N^2$: The alpha ocean is found where SCI > 1 immediately below the mixed layer, the beta ocean is where SCI < −1, while regions where −1 < SCI < 1 will be referred to as the transition zone. Alpha regions are associated with a thermocline, while beta regions feature a halocline. In the transition zone, both temperature and salinity contribute positively to the stratification.

Note that most of the ocean is either alpha or beta with a sharp transition, meaning that temperature and salinity stratifications are most often compensating each other (Fig. 2). For this reason, a large fraction of the global ocean is subject to double diffusion, either salt fingering (alpha) or diffusive (beta) (*15*), contributing to interior mixing. Figure 2C shows that the transition between the two regimes is generally found in the mid-latitudes, at a mean latitude of 50°N in both the Northern and Southern Hemispheres, although it can reach up to 80°N in the Nordic Seas. Note that an alternative definition for the separation between the three regimes has also been proposed on the basis of a statistical criterion (*16*).

The large TEC variations at the surface are dominated by changes in sea surface temperature (Fig. 2A). In the global ocean, the TEC varies from 0.3×10^{-4} °C^{-1} near the freezing temperature (≤0 ° C) to 3.5×10^{-4} °C^{-1} in tropical waters. In contrast, the saline contraction coefficient β varies by less than 10% in the ocean and can be considered constant to a good approximation. The temperature dependence of the TEC also induces the cabbeling or "densification upon mixing" effect in frontal regions (*17*, *18*). Note, however, that cabbeling is not a central focus of this work, as will be discussed more thoroughly in the last section.

A comparison between the global distributions of the TEC and SCI in the upper ocean indicates that beta regions correspond to relatively small TEC (Fig. 2). In this study, we investigate whether this correspondence is fortuitous or whether the decrease in TEC at low temperature is a key condition for the existence of beta regions in the ocean. This question cannot be addressed experimentally, as the equation of state (EOS) of seawater cannot be changed. The situation is, in this respect, analogous to the question of how a given bathymetric configuration constrains the observed circulation, which can only be investigated through theory and numerical simulations.

Forced ocean simulations (i.e., with imposed conditions at the surface boundary) have been performed in previous studies (*19*, *20*), which showed a large sensitivity of the global stratification distribution to changes in the TEC value, especially changes near the freezing point. However, the impact on sea ice was not realistic because forced simulations do not include atmospheric feedbacks. To avoid these unrealistic constraints, we use a fully coupled ocean–atmosphere–sea ice model with a simplified geometry (see Materials and Methods for details on the model configuration and sensitivity experiments). The nonlinear EOS implemented in the model will be replaced by a series of linear EOS with different TEC constant values, allowing us to investigate the sensitivity of the global climate to this water property.

RESULTS

The most marked changes observed when switching from a nonlinear to a linear EOS (at approximately constant global mean TEC) are

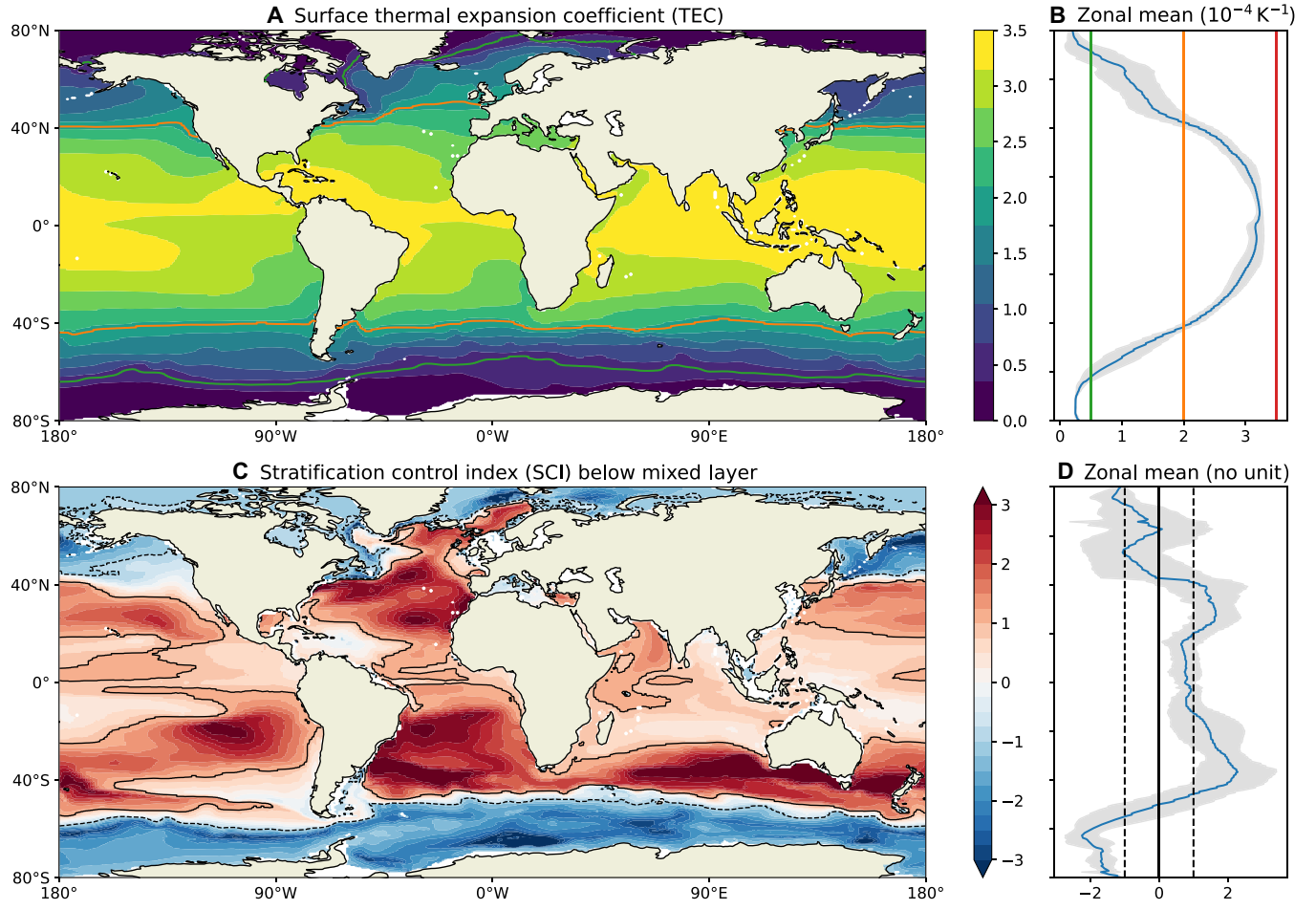

Fig. 2. Stratification control and surface TEC in the ocean. (**A**) Surface distribution of the TEC, showing a notable correlation with sea surface temperature. (**B**) Zonal-mean TEC showing an order of magnitude of var. (**C**) SCI (see core text for the definition). Blue, stratification dominated by salinity (beta regions); red, dominated by temperature (alpha regions). (**D**) Zonal-mean SCI. All figures are based on the Estimating the Circulation and Climate of the Ocean (ECCO) state estimate, version 4, release 4 (*66*). For each year, the SCI was computed on the layer found between 10 and 30 m below the mixed layer for the month of deepest mixed layer. The SCI distribution is obtained by averaging over the 21 years available in ECCO.

found in polar regions. While the control simulation Ctrl simulates a large ice pack in the Southern Hemisphere south of 60°S, the simulation Lin2.0 with a constant TEC value of 2.0×10^{-4} °C^{-1} is completely sea ice free (Fig. 3A; see also fig. S3). The sensitivity runs with linear EOS exhibit an abrupt regime transition between ice-free climates for large TEC and ice-covered poles for low TEC. The critical TEC value allowing the presence of sea ice is near 1.2×10^{-4} °C^{-1}. A constant value of about 0.8×10^{-4} °C^{-1} is required to produce the sea ice area found in Ctrl.

The surface and atmospheric responses to variations in TEC can be explained to a large extent by the changes in sea ice cover. A wider sea ice cover increases the planetary albedo, either directly or through changes in cloud cover, which not only tends to reduce the solar radiation absorbed at the surface (*21*) but also insulates the ocean from the atmosphere, allowing colder and drier conditions to develop in winter (*22*). The mean surface temperature increases rapidly (by about 2.5°C) with the disappearance of sea ice to stabilize just above 24°C in ice-free climates (Fig. 3B, blue).

Surface ocean forcings (fig. S5) are weakly affected by changes in TEC, with two notable exceptions. First, in polar regions and in the presence of sea ice, the strong divergence of fresh water from within the ice pack to its edge (due to equatorward spreading of ice) destabilizes the stratification and drives the formation of high-salinity bottom waters. In ice-free climates, the freshwater flux (due to net precipitation) stabilizes the stratification, but it is overcome by the destabilizing effect of the intense surface cooling that produces more widespread deep convection. Second, the surface heat flux is substantially modified in the mid-latitudes for the low-TEC run Lin0.5, reflecting fundamental differences in the structure of the overturning circulation with shallower overturning cells shifted equatorward (fig. S4). Changes in the Northern polar regions are less marked, probably because Ctrl had very little sea ice there to start with so surface fluxes are less likely to be modified.

Close inspection at zonal-mean temperature and salinity sections (Fig. 4) highlights the major impact that the value of TEC has on the ocean structure. For sufficiently high TEC values (2×10^{-4} to 3.5×10^{-4} °C^{-1}), the stratification in subtropical regions compares well with that of Ctrl (and the real ocean), with the characteristic W-shaped thermocline extending down to a similar depth of about 500 m. In the southern polar region, however, deep convection

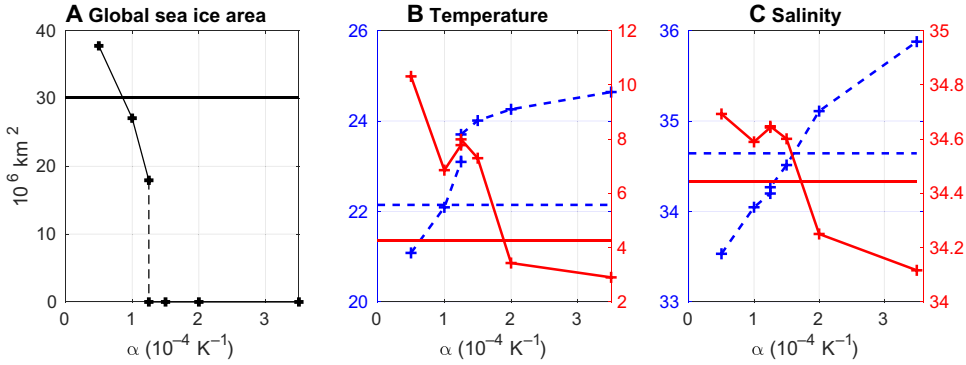

Fig. 3. Climate model sensitivity to different prescribed TECs. (**A**) Sea ice area, (**B**) sea surface temperature (0 to 40 m, blue) and bottom temperature (3000 to 4000 m, red), and (**C**) sea surface salinity (blue) and bottom salinity (red). Bottom values are averaged over the lowest kilometer (3000 to 4000 m), while surface values are averaged over the top 40 m. The horizontal lines denote the corresponding values in Ctrl.

becomes more vigorous at high TEC, and the stratification there nearly vanishes (Fig. 4, middle for Lin2.0). As a result, the southern polar surface becomes warmer/saltier and the bottom becomes cooler/fresher than in runs without convection. The spread of cold/fresh southern water masses results in lower bottom temperature globally (Fig. 3B, red) and a cooler global ocean, associated with a stronger deep overturning cell (fig. S4).

In contrast, at a low-TEC run (Lin0.5 in Fig. 4, C and F), deeper but weakly stratified thermoclines develop in both polar and subtropical regions. The abyssal ocean is filled with a warm water mass (10°C bottom temperature; Fig. 3B). This, as well as the absence of a subsurface salinity maximum in the subtropics, indicates the presence of salinity-driven convection in the subtropics. Overall, this run has weaker and less connected overturning cells, producing an essentially unventilated bottom ocean (fig. S4). The temperature contrast between surface and deep waters in the Southern Ocean is as large as 13°C, which is only possible due to the strong stabilizing effect of vertical salinity gradients.

The global mean sea surface salinity increases nearly linearly with the TEC (~1 g kg^{-1} for a unit 10^{-4} °C^{-1} of TEC; see Fig. 3C, blue). This is balanced by a freshening of the bottom ocean with increasing TEC, so as to satisfy global salt conservation in the ocean. The overall pattern of change is one of increasing contrast between the top and bottom of the ocean in both temperature and salinity (Fig. 3B). These temperature and salinity changes have opposite effects on the stabilization of the global stratification. As the temperature effect dominates (both the vertical temperature contrast and the impact of temperature on density increase with TEC), the top-to-bottom mean stratification strengthens for increasing values of TEC (Fig. 5).

The effect of the TEC on the stratification can be quantified by the SCI, which becomes systematically larger for higher values of TEC. In ice-free states, the thermal stratification N_T^2 is everywhere positive, indicating an inability to maintain cold waters near the surface while a salinity inversion ($N_S^2 < 0$, also seen in Ctrl) develops in the tropics and subtropics (corresponding to SCI > 1; Fig. 5C). In contrast, the low-TEC states have a marked temperature inversion in polar regions, as in Ctrl (see Fig. 4), but no salinity inversion in the subtropics, contrary to all the other simulations. The beta region (SCI < −1) in the low-TEC climates extends far into the subtropics up to 25° latitude, while the high-TEC climates do not exhibit beta regions at all.

It appears that the SCI in Ctrl closely matches at each latitude that the SCI value obtained in linear EOS simulations with the corresponding surface TEC. At high latitude where the TEC is low in Ctrl, the stratification resembles that of Lin0.5, while at low latitude, it resembles that of Lin2.0. This indicates that the TEC provides a strong constraint on the type of stratification that a particular location may experience. That is, the existence of distinct alpha and beta regions is primarily a consequence of the temperature dependence of the TEC of seawater.

Stratification below the sea ice

Our numerical experiments indicate the existence of a threshold in TEC above which sea ice cannot be sustained. The threshold value is between 1×10^{-4} and 1.5×10^{-4} °C^{-1} with a nonlinear transition, as a centennial oscillation between two unstable states is observed in Lin1.25 (see fig. S2). The quantitative prediction for the threshold value is likely model dependent and should be taken with caution. We argue, however, that the existence of such a threshold is expected and can be rationalized using the theoretical model of Martinson (*23*) for the stratification below sea ice.

The model considers a steady-state upper ocean and expresses the conservation of mass, salt, and heat. A central element is that, in the presence of sea ice, the surface layer is at the freezing point, which is the minimum possible temperature of seawater. This implies that the vertical gradient of temperature below sea ice is necessarily negative, $\partial_z \Theta \leq 0$.

To ensure static stability and a steady state, the total stratification N^2 must be positive, implying that the salinity stratification N_S^2 must be positive and large enough to compensate the temperature inversion or (see Eq. 2)

$$\beta \partial_z S \leq \alpha \partial_z \Theta \leq 0 \tag{3}$$

In the case of a freshwater lake ($\partial_z S = 0$), where $\alpha < 0$, the stability condition (Eq. 3) is satisfied unconditionally (recall, $\partial_z \Theta \leq 0$). In the saltwater ocean, however, the TEC is everywhere positive, so that $N_\Theta^2 \leq 0$ under the sea ice. There, the stratification must be salinity controlled, with $\partial_z S \leq 0$ (fresh water on top). This introduces an upper limit on the magnitude of the (negative) temperature gradient that can be maintained, which depends not only on the salinity gradient but also strongly on the TEC value.

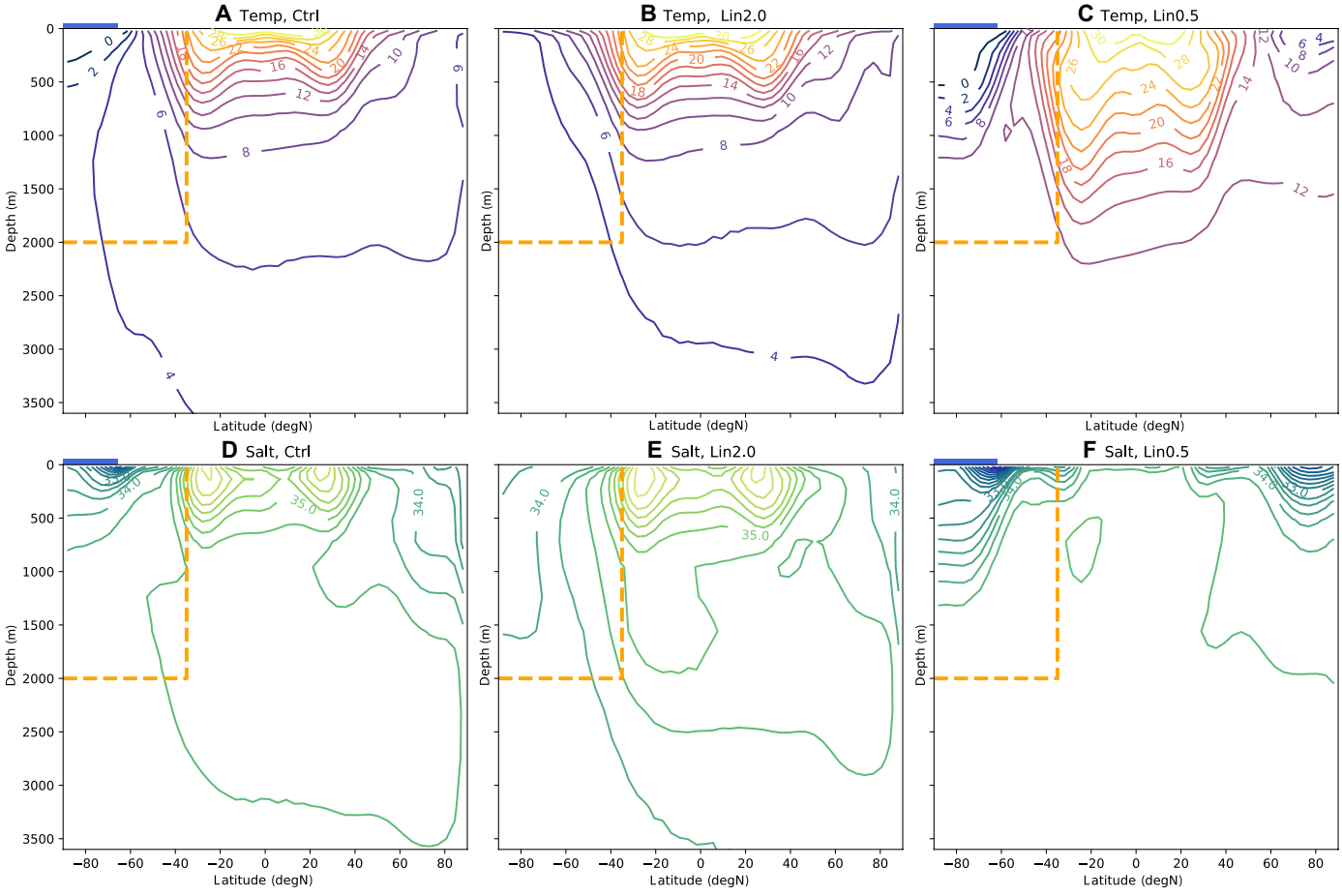

Fig. 4. Global modifications of the mean thermohaline stratification for different prescribed TECs. Zonally averaged sections of temperature (top) and salinity (bottom): (**A** to **D**) Ctrl, (**B** to **E**) Lin2.0, and (**C** to **F**) Lin0.5. Dashed orange lines in the top left corner denote the zonally reentrant section above the seal and south of the continents. Blue squares indicate the sea ice extent.

A critical value for the TEC can be obtained in the limit where the stratification would vanish

$$\alpha \leq \alpha_c = \frac{\beta \partial_z S}{\partial_z \Theta} \tag{4}$$

In a steady state, the gradient of salinity must be primarily controlled by the net rate of precipitation, which acts to stabilize the stratification. The surface cooling, which weakens the stability, may occur not only by air-sea/ice-sea interaction but also as a result of the ice melting needed to close the ice mass budget. Conservation of salt, mass, and heat requires compensating diffusive fluxes at the base of the mixed layer. Using simplified ice mass, heat, and salt budgets and assuming identical diffusivities for temperature and salinity, one finds an expression for the critical TEC α_c (see the Supplementary Materials for detailed derivations)

$$\alpha_c = \beta S_0 \frac{\rho_w c_p P}{Q + \rho_0 L_i A P}, \tag{5}$$

where P is the net precipitation (defined as precipitation minus evaporation plus river runoff), Q is the net surface heat flux, and A is the sea ice fraction (see table S1 for definitions of constants). A stable state with sea ice can only be maintained for a TEC value smaller than α_c. In polar regions where precipitation dominates evaporation ($P > 0$) and the ocean loses heat to the ice/atmosphere ($Q > 0$), α_c is positive. Equation 5 shows that, as expected, larger heat loss reduces α_c and the range of stability. The role of net precipitation P is more complex, appearing both in the numerator and denominator of Eq. 5. Larger precipitation stabilizes the water column by lowering the surface salinity, which permits a larger α_c (numerator). Simultaneously, larger precipitation over ice must be balanced by melting at the ice base and hence larger latent heat loss, which reinforces the destabilizing effect of Q (denominator).

For realistic values of the parameters (table S1), a critical value of $\alpha_c \approx 0.9 \times 10^{-4}$ °C^{-1} is obtained. Despite strong simplifications, this estimate is consistent with the TEC values where the transition to an ice-free climate occurs in the coupled model (Fig. 3). The fact that the critical TEC value is well below the global mean TEC value confirms that the conditions to form sea ice in the open ocean could not be met in the current Earth climate if the TEC value was not dropping at low temperature. Furthermore, it demonstrates that this water property, through (Eq. 5), imposes a constraint on the Earth's climate state.

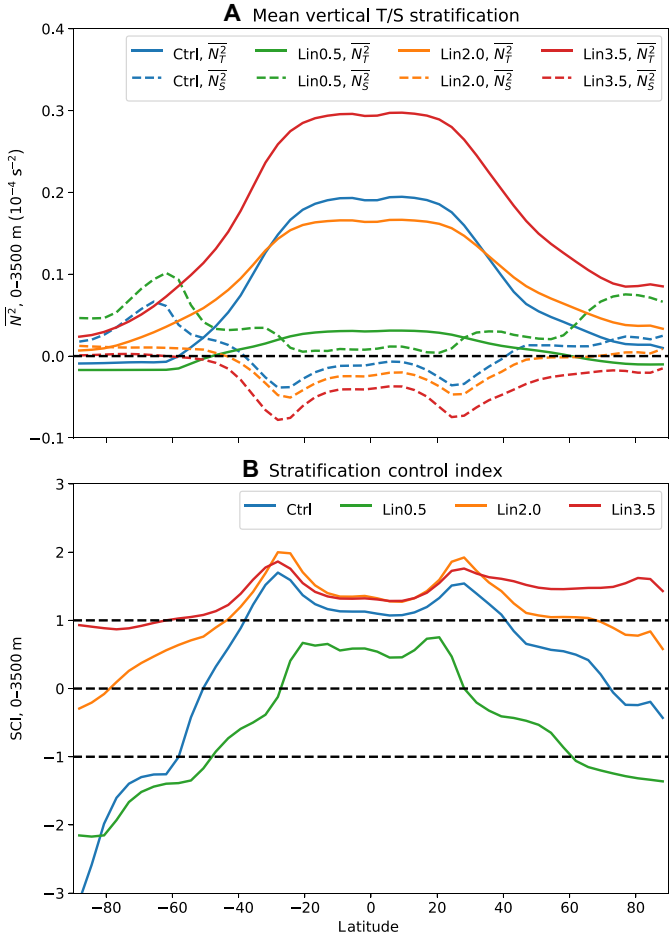

Fig. 5. Relative contributions of temperature and salinity on the stratification controlled by the TEC. (**A**) Zonally averaged haline (N_S^2) and thermal (N_Θ^2) buoyancy frequencies averaged from the surface to bottom, shown for the control run and the three sensitivity experiments. (**B**) SCI computed using vertically and zonally averaged buoyancy frequencies. The mean SCI of Ctrl compares well with that of Lin0.5 in polar regions, especially in the southern ice-covered domain, but is closer to that of Lin2.0 and Lin3.5 in subtropical regions. These variations in SCI are consistent with changes in surface TEC in Ctrl related to sea surface temperature changes.

DISCUSSION

Here, we have shown that the temperature dependence of the TEC is key to favoring the formation of a beta ocean (stratified by salinity) and largely controls the sea ice extent using a range of coupled ocean-atmosphere simulations. It was further shown that, even if a net freshwater flux in polar regions is necessary to form a halocline, it is not enough to maintain the beta stratification stable in the presence of intense surface cooling except maybe in geographically limited cold estuarine regions. Sea ice formation has long been noted to require beta ocean conditions to occur away from shallow areas (*13*, *24*). The idea that a reduction of the TEC in the cold high latitudes could promote sea ice formation was even suggested (*13*, *20*, *25*), and it is demonstrated here.

The transition from alpha to beta stratification is not caused by cabbeling, contrary to previous suggestions (*13*). Cabbeling, also known as densification upon mixing, generates a convergence across the frontal boundaries as isopycnal mixing in the interior acts to densify seawater (*26*, *27*). Rates of cabbeling depend on how fast the TEC varies with temperature; however, they also require a combination of eddy stirring and molecular diffusion to generate the convergence. That cabbeling may increase the abruptness of the transition from alpha to beta cannot be entirely discarded here; however, our results based on linear EOS simulations (thus entirely free of cabbeling by construct) show that cabbeling is not necessary for the existence of these transitions (Fig. 5).

This is consistent with recent numerical experiments showing that the transition zone in polar regions is set by an inversion of the mean surface buoyancy flux, linked to the drop in polar TEC value at low temperature (*28*) rather than cabbeling. This temperature dependence of the TEC should also imply a weaker and more indirect role of the wind forcing on the position of fronts than previously hypothesized (*29*). The position of the transition zone can, however, be influenced by changes in the strength of the halocline, which can be driven by hydrological changes (*30*), ice shelf melting (*31*), or wind anomalies (*32*). This points toward a subtle, nonlinear interplay between heat and freshwater surface fluxes in controlling the meridional structure of the upper ocean stratification.

The idea that the TEC might have a global influence on the climate is, of course, not entirely new although not always explicitly acknowledged. Experiments using global atmosphere/ocean general circulation models can be found in the literature, where the global mean salinity (*33*, *34*) or the global mean temperature (*35*) of the simulated ocean is artificially modified, indirectly modifying the thermohaline range of water masses and, consequently, the way the TEC varies with temperature. Our simulations show that increased TEC values in the polar region, as may be found in warmer climates, are associated with colder and fresher deep water properties (Fig. 3). The ventilation is expected to be stronger in warm climates than in cold climates, as the polar halocline necessitates temperature near the freezing point to be maintained (*36*). This, in turn, may induce an anticorrelation between the global mean temperature and the carbon storage in the deep ocean, further amplifying climate changes. This mechanism has been suggested to explain the transition to the Pleistocene cycle of ice ages, 2.7 million years ago (*37*). This may also explain why salinity forcing seems to dominate during the Last Glacial Maximum, simply because it was in a colder state (*38*).

The large sensitivity of the global ocean structure and sea ice formation to the TEC highlighted here has strong implications for how the ocean may respond to a climate change. If the position of the polar transition zone is controlled by the value of the TEC, itself mostly a function of the sea surface temperature, migrations of the transition zone between alpha and beta regions should be largely driven by the surface heat fluxes. This appears consistent with the current "atlantification" of the Eurasian Arctic basin, caused by a warming of the Atlantic inflows and producing a northward migration of the transition zone and a concurrent shrinking of the sea ice extent (*39*). On the other hand, the idea of an increased ventilation in a warmer climate (*35*, *36*) somewhat contradicts the common inference that global warming may induce a slowdown and even possibly a collapse of the Atlantic Meridional Overturning Circulation (*40*). The competing effects of freshening and warming in shifting the stratification control, particularly in the Nordic Seas (*41*, *42*), need to be better understood to predict how polar climate changes affect the ventilation and overturning rates.

Our simulation with a uniform TEC corresponding to the present-day global ocean value ($\alpha = 2.0 \times 10^{-4}$ °C^{-1}) is warmer than the

control simulation by about 2°C and is totally ice free. Depending on estimates of the climate sensitivity (*43*), a decrease in atmospheric CO_2 by a factor of about 2 to 5 would be necessary to form sea ice with this uniform TEC (see the Supplementary Materials). All things equal (concentration of CO_2 and other greenhouse gas, solar constant, continental distribution, etc.), the unique variation of the water TEC greatly facilitates the growth of sea ice, with a cascading impact on global climate conditions. For example, by affecting the stratification and rates of transport of essential nutrients such as phosphate, variations of seawater's TEC constrain the ocean productivity (with feedbacks on the global carbon cycle), making it potentially relevant to habitability conditions in the presence of an ocean (*44*). These exoplanets that have attracted a lot of attention as salty (e.g., the presence of nutrient) oceans, in addition to being a favorable medium to harbor life, can significantly moderate climate response to changing astronomical parameters and therefore widen the habitable zone (*45*).

Our study highlights that estimates of habitable zone should avoid simplified linear EOS with constant TEC (*34*, *46*). As shown by our simulations, neglecting the unique thermal expansion properties of seawater may significantly overestimate the global mean temperature and therefore underestimate the possibilities of a descent into global glaciation with potential relevance to the transition toward and from snowball states (*47*, *48*). Also, salinity of oceans may vary markedly over time (*49*) and between planets (*50*), affecting the thermal sensitivity of the global ocean. Exploration of the full range of salinity and their climate impact will require to account for the full nonlinearity of the seawater EOS.

MATERIALS AND METHODS

Description of the climate model

Simulations are carried out with the MIT General Circulation Model (*51*), which solves for the three-dimensional circulation of atmosphere and ocean and includes sea ice and land surface processes. The atmospheric physics is of "intermediate" complexity based on SPEEDY (*52*) at low vertical resolution (further details in the Supplementary Materials). The configuration comprises two land-barrier masses defining a narrow Atlantic-like basin and a wide Pacific-like basin connecting to an unblocked Southern Ocean. Despite its simplified geometry, the configurations include many of the essential dynamics that shape Earth's climate system (e.g., hydrological cycle and storm tracks) (*53*). It also captures two key asymmetries: an asymmetry between the two northern basins with the absence of deep water formation in the Pacific Ocean (*54*) and a north-south asymmetry between wind-driven gyres in the north and a vigorous Southern Ocean circumpolar current.

The barrier to the west of the small basin (analogous to the American continent) is extended with a submarine ridge between 2000 and 4000 m in depth. This allows a northward propagation of bottom water produced in the south and a more realistic representation of the bottom meridional cell than in previous reported simulations (*54*). Furthermore, a maximum sea ice concentration of 90% is set in the model, and an ice thickness diffusion is applied to prevent the formation of ice caps that completely insulate the ocean from the atmosphere and ensure a more realistic production of bottom waters in ice-covered areas.

In its reference configuration, the coupled model uses the standard EOS-80 for salty water, with potential temperature and practical salinity as prognostic variables (*4*). However, following recent recommendations (*55*), we will nonetheless interpret them as conservative temperature (a quantity proportional to potential enthalpy with units of temperature) and absolute salinity (the grams of solute per kilogram of seawater), respectively. Note that quantitative discrepancies between thermodynamic standards are small (<1%) and are not susceptible to modify the conclusions here.

Design of the sensitivity experiments

To test the sensitivity of the climate to the TEC value, we implement a linear EOS approximation

$$\rho_{\mathrm{model}} = \rho_0(1 - \alpha_0 \Theta + \beta_0 S) \tag{6}$$

where α_0, β_0, and ρ_0 are uniform globally. Having a linear EOS enables us to investigate the effect of the TEC value at different latitudes while keeping the analysis simple. We chose not to include a nonlinear term in the EOS, despite their potential impact on the global water mass distribution through cabbeling or thermobaricity effects (*19*), to better isolate the local impact of the TEC value on the surface buoyancy forcings and on the upper stratification.

We carry out the following experiments, which only differ by their EOS:

1) Ctrl: Control simulation with the nonlinear EOS-80; spin up of 9 thousand years (ka).

2) Lin2.0: Simulation with the linear EOS with $\alpha_0 = 2.0 \times 10^{-4}\,°\mathrm{C}^{-1}$. The simulation is initialized from the end state of Ctrl and then run for 7 ka.

3) Lin0.5, Lin1.0, Lin1.25 and Lin1.5, and Lin3.5: Simulations with linear EOS with $\alpha_0 = 0.5$, 1.0, 1.25, 1.5, and 3.5 in units of $10^{-4}\,°\mathrm{C}^{-1}$, respectively. These simulations are branched off from the end state of Lin2.0 and run for a minimum of 5 ka.

Note that the globally averaged TEC values in Ctrl (nonlinear EOS) and Lin2.0 (linear EOS) are very similar. The haline contraction coefficient is set to the constant $\beta_0 = 7.8 \times 10^{-4}\,(\mathrm{g/kg})^{-1}$. The time series of the sea surface temperature and sea ice area are shown in figs. S1 and S2. Illustrations below use the past 50 years of each simulation.

SUPPLEMENTARY MATERIALS

Supplementary material for this article is available at https://science.org/doi/10.1126/sciadv.abq0793

REFERENCES AND NOTES

1. Y. Maréchal, *The hydrogen bond and the water molecule: The physics and chemistry of water, aqueous and bio media* (Elsevier, 2007).
2. D. L. Hartmann, *Global Physical Climatology* (Newnes, 2015), vol. 103.
3. D. Eisenberg, W. Kauzmann, *The Structure and Properties of Water* (Oxford Univ. Press on demand, 2005).
4. IOC and SCOR and IAPSO, The international thermodynamic equation of seawater – 2010: Calculation and use of thermodynamic properties., Intergovernmental Oceanographic Commission, Manuals and Guides No. 56, UNESCO (English) (2010), 196 p.
5. T. S. Ingebrigtsen, T. B. Schrøder, J. C. Dyre, What is a simple liquid? *Phys. Rev. X* **2**, 011011 (2012).
6. A. Van Itterbeek, O. Verbeke, Density of liquid nitrogen and argon as a function of pressure and temperature. *Physica* **26**, 931–938 (1960).
7. G. E. Hutchinson, H. Löffler, The thermal classification of lakes. *Proc. Natl. Acad. Sci. U.S.A.* **42**, 84–86 (1956).
8. W. M. Lewis Jr., A revised classification of lakes based on mixing. *Can. J. Fish. Aquat. Sci.* **40**, 1779–1787 (1983).

9. B. Boehrer, Thermobaric Stratification of Very Deep Lakes, in *Encyclopedia of Lakes and Reservoirs*, L. Bengtsson, R. W. Herschy, R. W. Fairbridge, Eds. (Encyclopedia of Earth Sciences Series, Springer Netherlands, 2012), pp. 800–801.
10. R. Mancinelli, A. Botti, F. Bruni, M. Ricci, A. Soper, Perturbation of water structure due to monovalent ions in solution. *Phys. Chem. Chem. Phys.* **9**, 2959–2967 (2007).
11. V. Pellichero, J.-B. Sallée, S. Schmidtko, F. Roquet, J.-B. Charrassin, The ocean mixed layer under southern ocean sea-ice: Seasonal cycle and forcing. *J. Geophys. Res. Oceans* **122**, 1608–1633 (2017).
12. E. C. Carmack, M. Yamamoto-Kawai, T. W. N. Haine, S. Bacon, B. A. Bluhm, C. Lique, H. Melling, I. V. Polyakov, F. Straneo, M. L. Timmermans, W. J. Williams, Freshwater and its role in the arctic marine system: Sources, disposition, storage, export, and physical and biogeochemical consequences in the arctic and global oceans. *J. Geophys. Res. Biogeosc.* **121**, 675–717 (2016).
13. E. C. Carmack, The alpha/beta ocean distinction: A perspective on freshwater fluxes, convection, nutrients and productivity in high-latitude seas. *Deep Sea Res. Part II Top. Stud. Oceanogr.* **54**, 2578–2598 (2007).
14. G. K. Vallis, *Atmospheric and oceanic fluid dynamics* (Cambridge Univ. Press, 2012).
15. R. W. Schmitt, Double diffusion in oceanography. *Annu. Rev. Fluid Mech.* **26**, 255–285 (1994).
16. K. D. Stewart, T. W. N. Haine, Thermobaricity in the transition zones between alpha and beta oceans. *J. Phys. Oceanogr.* **46**, 1805–1821 (2016).
17. T. J. McDougall, Thermobaricity, cabbeling, and water-mass conversion. *J. Geophys. Res. Oceans* **92** (C5), 5448–5464 (1987).
18. S. Groeskamp, R. P. Abernathey, A. Klocker, Water mass transformation by cabbeling and thermobaricity. *Geophys. Res. Lett.* **43**, 10835–10845 (2016).
19. J. Nycander, M. Hieronymus, F. Roquet, The nonlinear equation of state of sea water and the global water mass distribution. *Geophys. Res. Lett.* **42**, 7714–7721 (2015).
20. F. Roquet, G. Madec, L. Brodeau, J. Nycander, Defining a simplified yet "realistic" equation of state for seawater. *J. Phys. Oceanogr.* **45**, 2564–2579 (2015).
21. D. Rind, R. Healy, C. Parkinson, D. Martinson, The role of sea ice in $2\times CO_2$ climate model sensitivity. Part I: The total influence of sea ice thickness and extent. *J. Climate* **8**, 449–463 (1995).
22. S. Manabe, R. T. Wetherald, The effects of doubling the CO_2 concentration on the climate of a general circulation model. *J. Atmos. Sci.* **32**, 3–15 (1975).
23. D. G. Martinson, Evolution of the southern ocean winter mixed layer and sea ice: Open ocean deepwater formation and ventilation. *J. Geophys. Res. Oceans* **95**, 11641–11654 (1990).
24. N. P. Bulgakov, The role of convection in the mechanism of heat transfer of deep atlantic water, in *Deep Sea Res. and Oceanographic Abstracts* (1962), vol. 9, pp. 233–239.
25. C. Rooth, Hydrology and ocean circulation. *Prog. Oceanogr.* **11**, 131–149 (1982).
26. A. Klocker, T. J. McDougall, Influence of the nonlinear equation of state on global estimates of dianeutral advection and diffusion. *J. Phys. Oceanogr.* **40**, 1690–1709 (2010).
27. S. Groeskamp, R. P. Abernathey, A. Klocker, Water mass transformation by cabbeling and thermobaricity. *Geophys. Res. Lett.* **43**, 10835–10845 (2020).
28. R. Caneill, F. Roquet, G. Madec, J. Nycander, The polar transition from alpha to beta regions set by a surface buoyancy flux inversion. *J. Phys. Oceanogr.* **52**, 1887–1902 (2022).
29. J. R. Toggweiler, Shifting westerlies. *Science* **323**, 1434–1435 (2009).
30. P. J. Durack, S. E. Wijffels, R. J. Matear, Ocean salinities reveal strong global water cycle intensification during 1950 to 2000. *Science* **336**, 455–458 (2012).
31. E. Rignot, S. Jacobs, J. Mouginot, B. Scheuchl, Ice-shelf melting around antarctica. *Science* **341**, 266–270 (2013).
32. S. R. Rintoul, M. H. England, Ekman transport dominates local air-sea fluxes in driving variability of subantarctic mode water. *J. Phys. Oceanogr.* **32**, 1308–1321 (2002).
33. P. D. Williams, E. Guilyardi, G. Madec, S. Gualdi, E. Scoccimarro, The role of mean ocean salinity in climate. *Dyn. Atmospheres Oceans* **49**, 108–123 (2010).
34. J. Cullum, D. P. Stevens, M. M. Joshi, Importance of ocean salinity for climate and habitability. *Proc. Natl. Acad. Sci. U.S.A.* **113**, 4278–4283 (2016).
35. A. M. de Boer, D. M. Sigman, J. R. Toggweiler, J. L. Russell, Effect of global ocean temperature change on deep ocean ventilation. *Paleoceanography* **22**, PA2210 (2007).
36. M. Winton, The effect of cold climate upon north atlantic deep water formation in a simple ocean-atmosphere model. *J. Climate* **10**, 37–51 (1997).
37. D. M. Sigman, S. L. Jaccard, G. H. Haug, Polar ocean stratification in a cold climate. *Nature* **428**, 59–63 (2004).
38. J. F. Adkins, K. McIntyre, D. P. Schrag, The salinity, temperature, and δ18O of the glacial deep ocean. *Science* **298**, 1769–1773 (2002).
39. I. V. Polyakov, A. V. Pnyushkov, M. B. Alkire, I. M. Ashik, T. M. Baumann, E. C. Carmack, I. Goszczko, J. Guthrie, V. V. Ivanov, T. Kanzow, R. Krishfield, R. Kwok, A. Sundfjord, J. Morison, R. Rember, A. Yulin, Greater role for Atlantic inflows on sea-ice loss in the Eurasian Basin of the Arctic Ocean. *Science* **356**, 285–291 (2017).
40. W. Weijer, W. Cheng, S. S. Drijfhout, A. V. Fedorov, A. Hu, L. C. Jackson, W. Liu, E. L. McDonagh, J. V. Mecking, J. Zhang, Stability of the atlantic meridional overturning circulation: A review and synthesis. *J. Geophys. Res. Oceans* **124**, 5336–5375 (2019).
41. C. Lique, M. D. Thomas, Latitudinal shift of the Atlantic meridional overturning circulation source regions under a warming climate. *Nat. Clim. Chang.* **8**, 1013–1020 (2018).
42. M. S. Lozier, F. Li, S. Bacon, F. Bahr, A. S. Bower, S. A. Cunningham, M. F. de Jong, L. de Steur, B. de Young, J. Fischer, S. F. Gary, B. J. W. Greenan, N. P. Holliday, A. Houk, L. Houpert, M. E. Inall, W. E. Johns, H. L. Johnson, C. Johnson, J. Karstensen, G. Koman, I. A. le Bras, X. Lin, N. Mackay, D. P. Marshall, H. Mercier, M. Oltmanns, R. S. Pickart, A. L. Ramsey, D. Rayner, F. Straneo, V. Thierry, D. J. Torres, R. G. Williams, C. Wilson, J. Yang, I. Yashayaev, J. Zhao, A sea change in our view of overturning in the subpolar North Atlantic. *Science* **363**, 516–521 (2019).
43. M. D. Zelinka, T. A. Myers, D. T. McCoy, S. Po-Chedley, P. M. Caldwell, P. Ceppi, S. A. Klein, K. E. Taylor, Causes of higher climate sensitivity in CMIP6 models. *Geophys. Res. Lett.* **47**, e2019GL085782 (2020).
44. S. L. Olson, M. Jansen, D. S. Abbot, Oceanographic considerations for exoplanet life detection. *Astrophys. J.* **895**, 19 (2020).
45. D. Ferreira, J. Marshall, P. A. O'Gorman, S. Seager, Climate at high-obliquity. *Icarus* **243**, 236–248 (2014).
46. K. M. Soderlund, B. E. Schmidt, J. Wicht, D. D. Blankenship, Ocean-driven heating of europa's icy shell at low latitudes. *Nat. Geosci.* **7**, 16–19 (2014).
47. P. F. Hoffman, D. P. Schrag, The snowball Earth hypothesis: Testing the limits of global change. *Terra Nova* **14**, 129–155 (2002).
48. P. F. Hoffman, D. S. Abbot, Y. Ashkenazy, D. I. Benn, J. J. Brocks, P. A. Cohen, G. M. Cox, J. R. Creveling, Y. Donnadieu, D. H. Erwin, I. J. Fairchild, D. Ferreira, J. C. Goodman, G. P. Halverson, M. F. Jansen, G. le Hir, G. D. Love, F. A. Macdonald, A. C. Maloof, C. A. Partin, G. Ramstein, B. E. J. Rose, C. V. Rose, P. M. Sadler, E. Tziperman, A. Voigt, S. G. Warren, Snowball earth climate dynamics and cryogenian geology-geobiology. *Sci. Adv.* **3**, e1600983 (2017).
49. L. P. Knauth, Salinity history of the earth's early ocean. *Nature* **395**, 554–555 (1998).
50. S. N. Raymond, T. Quinn, J. I. Lunine, Making other earths: Dynamical simulations of terrestrial planet formation and water delivery. *Icarus* **168**, 1–17 (2004).
51. J. Marshall, A. Adcroft, C. Hill, L. Perelman, C. Heisey, A finite-volume, incompressible navier stokes model for studies of the ocean on parallel computers. *J. Geophys. Res. Oceans* **102**, 5753–5766 (1997).
52. F. Molteni, Atmospheric simulations using a GCM with simplified physical parametrizations. I: Model climatology and variability in multi-decadal experiments. *Climate Dynam.* **20**, 175–191 (2003).
53. D. Ferreira, J. Marshall, J.-M. Campin, Localization of deep water formation: Role of atmospheric moisture transport and geometrical constraints on ocean circulation. *J. Climate* **23**, 1456–1476 (2010).
54. D. Ferreira, P. Cessi, H. K. Coxall, A. de Boer, H. A. Dijkstra, S. S. Drijfhout, T. Eldevik, N. Harnik, J. F. McManus, D. P. Marshall, J. Nilsson, F. Roquet, T. Schneider, R. C. Wills, Atlantic-pacific asymmetry in deep water formation. *Annu. Rev. Earth Planet. Sci.* **46**, 327–352 (2018).
55. T. J. McDougall, P. M. Barker, R. M. Holmes, R. Pawlowicz, S. M. Griffies, P. J. Durack, The interpretation of temperature and salinity variables in numerical ocean model output and the calculation of heat fluxes and heat content. *Geosci. Model Dev.* **14**, 6445–6466 (2021).
56. J. Marshall, C. Hill, L. Perelman, A. Adcroft, Hydrostatic, quasi-hydrostatic, and nonhydrostatic ocean modeling. *J. Geophys. Res. Oceans* **102**, 5733–5752 (1997).
57. J. Marshall, A. Adcroft, J.-M. Campin, C. Hill, A. White, Atmosphere-ocean modeling exploiting fluid isomorphisms. *Mon. Wea. Rev.* **132**, 2882–2894 (2004).
58. A. Adcroft, J.-M. Campin, Re-scaled height coordinates for accurate representation of free-surface flows in ocean circulation models. *Ocean Model.* **7**, 269–284 (2004).
59. A. Adcroft, J. Campin, C. Hill, J. Marshall, Implementation of an atmosphere-ocean general circulation model on the expanded spherical cube. *Mon. Wea. Rev.* **132**, 2845–2863 (2004).
60. J.-M. Campin, J. Marshall, D. Ferreira, Sea ice-ocean coupling using a rescaled vertical coordinate *z*. *Ocean Model.* **24**, 1–14 (2008).
61. P. R. Gent, J. C. McWilliams, Isopycnal mixing in ocean circulation models. *J. Phys. Oceanogr.* **20**, 150–155 (1990).
62. M. H. Redi, Oceanic isopycnal mixing by coordinate rotation. *J. Phys. Oceanogr.* **12**, 1154–1158 (1982).
63. B. A. Klinger, J. Marshall, U. Send, Representation of convective plumes by vertical adjustment. *J. Geophys. Res. Oceans* **101**, 18175–18182 (1996).
64. M. Winton, A reformulated three-layer sea ice model. *J. Atmos. Oceanic Tech.* **17**, 525–531 (2000).

65. G. Myhre, E. J. Highwood, K. P. Shine, F. Stordal, New estimates of radiative forcing due to well mixed greenhouse gases. *Geophys. Res. Lett.* **25**, 2715–2718 (1998).
66. G. Forget, J. M. Campin, P. Heimbach, C. N. Hill, R. M. Ponte, C. Wunsch, ECCO version 4: An integrated framework for non-linear inverse modeling and global ocean state estimation. *Geosci. Model Dev.* **8**, 3071–3104 (2015).

Acknowledgments
Funding: No funding was required for this work. **Author contributions:** F.R. initiated the project. D.F. performed numerical runs and helped with their analysis. R.C. carried out analysis of the Estimating the Circulation and Climate of the Ocean (ECCO) product. D.S. contributed with his expertise in chemical physics of water. G.M. provided important inputs in interpreting the results. F.R. wrote the initial draft. All authors contributed to the final manuscript. **Competing interests:** The authors declare that they have no competing interests. **Data and materials availability:** All data needed to evaluate the conclusions in the paper are present in the paper and/or the Supplementary Materials. Model data supporting the results reported here are openly available from the University of Reading Research Data Archive at https://doi.org/10.17864/1947.000394.

Submitted 16 March 2022
Accepted 23 September 2022
Published 16 November 2022
10.1126/sciadv.abq0793